ELSEVIER

Physica C 242 (1995) 99–104

PHYSICA C

Fabrication and characterization of YBCO Josephson junctions based on artificially generated bi-epitaxial grain boundary

S. Nicoletti [a,1,*], H. Moriceau [a], J.C. Villegier [a], D. Chateigner [b]

[a] *LETI (CEA – Technologies Avancées) DOPT/SCCM-CEN/G-17, Av. des Martyrs, 38054 Grenoble Cedex 09, France*
[b] *CNRS-Laboratoire de Cristallographie, BP, 38040 Grenoble Cedex 09, France*

Received 10 August 1994

Abstract

In this paper we report the thin-film in-plane fabrication and the structural characterization of artificially engineered grain boundaries obtained by partly interposing an MgO seed layer between the $SrTiO_3$ (STO) substrate and the CeO_2 buffer layer. X-ray pole figures show that films grown onto the seed layer are slightly disordered with respect to the remaining part of the sample. The junctions, realized by patterning the grain boundary occurring in the overhanging YBCO film show Josephson current modulation in a large temperature range with an I_cR_n value of about 230 μV at 9 K, the R_n value being constant over the whole superconducting region. Under microwave irradiation, the I–V characteristics display several Shapiro steps while in accordance with the resistively shunted junction (RSJ) behavior, the step heights have the typical current-biased junction dependence.

1. Introduction

The developing of superconducting electronics actually represents one of the most promising applications of high-temperature superconductor (HTS) materials. In realizing this aim, the realization of reproducible Josephson junctions (JJ) represents one of the most important milestones in the developing of superconducting electronics.

Due to the short coherence length of HTS materials, the device-fabrication procedure using in-situ "trilayers" technology used for low-temperature conventional superconductors cannot be easily implemented in the case of HTS materials. On the other hand, the realization of JJ based on *a*-oriented multilayered structures requires at least two superconducting layers and a structurally matched, chemically stable intermediate barrier film. Even if this kind of structure has been already obtained [3,4], the degree of complexity in the stacking sequence as well as the problems due to the injection of the junction current through *a*-oriented YBCO electrodes affect the reliability of this process.

Nevertheless, large-angle grain boundaries (GB's) are well known to behave like a weak link [5,6]. To develop artificially generated grain-boundary junctions (GBJ's), superconducting thin films were at first deposited on bi-crystal substrates [7,8]. The reproducibility of the obtained JJ makes this technique suitable to study the electrical behavior of GBJ based devices, but the integration in any large-scale technological process seems to be difficult. To avoid these restrictions, other approaches have been explored. Among the others, the realization of artificially engi-

* Corresponding author.
[1] Permanent address: CNR-Istituto LAMEL Via Gobetti, 101 I-40129 Bologna, Italy.

SSDI 0921-4534(94)00570-2

neered bi-epitaxial structures represents one of the most promising techniques [9–11]. The main peculiarity of bi-epitaxy can be summarized in the present capability to locate and engineer a single 45° tilted GB at any stage of the device preparation. This feature, as well as the typical current densities of about 10^2–10^3 A/cm^2 at 77 K, makes this technique suitable for many applications and for the realization of complex structures where different layers or collective arrays are required. However, for practical applications, the reliability and the reproducibility still remain the foremost issue in the fabrication of the devices. To this end, the understanding of the growth mechanism at the interface between substrate and seed layer as well as between the seed and buffer layers represents a crucial point for the reproducibility of devices based on bi-epitaxial grain boundaries.

This paper reports the fabrication and the characterization of Josephson junctions based on artificially engineered grain boundaries obtained by depositing a YBCO/CeO_2/MgO–YBCO/CeO_2 structure (hereafter referred to as YCM/YC) on a (100) oriented STO substrate. We investigated the role of the structural disorder occurring in the superconducting film under which the MgO seed layer is present. The presence of inhomogeneities occurring at the GB and their relevance on the electrical properties of the fabricated devices are discussed.

2. Experimental

To fabricate artificially engineered bi-epitaxial grain boundaries an MgO seed layer and a CeO_2 buffer layer were first deposited onto a (100) oriented STO substrate by pulsed-laser ablation. Film depositions have been realized in a multitarget system allowing for the subsequent growth of different layers without vacuum breaking. A detailed description of the deposition apparatus was reported elsewhere [12]. Then, these two intermediate layers were removed on part of the substrate by Ar ion milling of a photolithographically defined geometry, providing a smooth and sharp interface where the grain boundary will be located. A CeO_2 buffer and a YBCO superconducting layer were finally deposited onto the patterned substrate. Table 1 summarizes the parameters employed during each deposition step.

Table 1
Processing parameters used during seed, buffer and superconducting layers deposition

Film	MgO	CeO_2	CeO_2	YBCO
Target	Mg	CeO_2	CeO_2	YBCO
Energy (J/cm^2)	2.6	2.0	2.0	2.0
Rate (nm/shot)	9.5×10^{-3}	0.06	0.06	0.055
O_2 Pressure (Pa)	2.6	40	40	65
Dep. Temp. (°C)				
Thickness (nm)	600	780	780	750
	10	15	15	200

The obtained films were structurally characterized by X-ray diffraction analysis (XRD). Texture analyses were carried out on a four circle goniometer in the Schulz reflection geometry [13]. In the apparatus the radiation emitted from a rotating copper target was monochromatized and collimated giving a final beam dimension of 0.84×0.60 mm^2, the divergence being 0.28° and 0.23°, respectively. The pole figures were taken by scanning the tilt angle χ between 0° and 72° and the azimuthal angle φ between 0° and 360°. In order to detect very strong texture, steps of 0.9° were employed on both the rotations. For a collecting time of 1 s, the system provides in this configuration an ultimate resolution better than 0.1% in volume. The data were corrected for the background and for the defocusing and drawn by using our own program [14] (Cortexg and Pofint).

The electrical characterization was performed onto 10 μm wide and 200 μm long stripes defined across the GB by standard photolithographic technique. The YBCO film was, at last, patterned into the appropriate geometry by Ar ion milling at 500 eV. The obtained devices were placed onto a cryogenic probe and tested down to the liquid helium temperature in a μ-metal shielded dewar.

3. Results and discussion

In the following we refer to a series of samples grown under the conditions reported in Table 1. The results obtained do not differ significantly from sample to sample giving evidence of the reproducibility of the process itself.

3.1. XRD analyses

Fig. 1 displays a classical diffraction pattern of an YCM/YC structure. A strong preferred orientation of the YBCO layer with the *c*-axes perpendicular to the sample surface (S) is clearly shown. Even if the presence of the YBCO reduces the intensity of reflections emerging from the buffer layers, the appearance of the $(200)_{CeO_2}$, $(400)_{CeO_2}$ and $(200)_{MgO}$ peaks in this spectrum denotes a $\langle 001 \rangle$ main orientation for both films. Some $BaCeO_3$ impurities, detected by their (112+200) reflections, are also present in minor amount. The presence of such a precipitate can be attributed to some interfacial reactions between the superconducting film and the buffer layer [15].

Figs. 2(a) and (b) shows the $\{111\}_{CeO_2}$ and $\{115\}_{YBCO}$ pole figures, respectively. In both diffractograms we can identify two different sets of poles, 45° rotated one with respect to the other, giving evidence of two in-plane orientations of the crystallites. The same investigation performed on two different samples with and without the MgO seed layer detects only one set of peaks, revealing that the following in-plane relationships are peculiarities of each stacking sequence. In the CeO_2 pole figure the peaks, located on a ring at $\chi = 55°$, obey the heteroepitaxial relations

$$a_{\perp 0}^{CeO_2}: \begin{cases} \langle 100 \rangle_{CeO_2} \| (MgO) \| \langle 100 \rangle_{STO}, \\ \langle 001 \rangle_{CeO_2} \| \langle 001 \rangle_{MgO} \| \langle 001 \rangle_{STO}, \end{cases}$$

$$a_{\perp 45}^{CeO_2}: \begin{cases} \langle 100 \rangle_{CeO_2} \| \langle 110 \rangle_{STO}, \\ \langle 001 \rangle_{CeO_2} \| \langle 001 \rangle_{STO}, \end{cases}$$

for the YCM and YC part of the sample, respectively. The width extension of each peak, taken at 15% of the maximal intensity, is about 5° and 10° in φ and in χ, respectively. On the other hand, by integrating over each group of peaks and averaging per unit volume, we found a relative ratio $a_{\perp 0}^{CeO_2}/a_{\perp 45}^{CeO_2} = 0.28$ denoting a low degree of crystal perfection in the CeO_2 film on the MgO seed layer.

The occurrence of this eight-fold symmetry has to be attributed to the presence of an MgO seed layer between the substrate surface and the CeO_2 buffer layer. Where the seed layer is present the buffer CeO_2 layer grows following the "cube-on-cube" relation (i.e. 0° in-plane rotation) while, elsewhere on STO, the CeO_2 cells are 45° rotated with respect to those of the substrate. This behavior, widely reported in the literature [9,15], allows for the realization of engineered grain boundaries occurring at the edge of a region where an MgO seed layer is deposited.

The $\{115\}_{YBCO}$ pole figure shown in Fig. 2(b) reveals strong in-plane orientation of the YBCO layer.

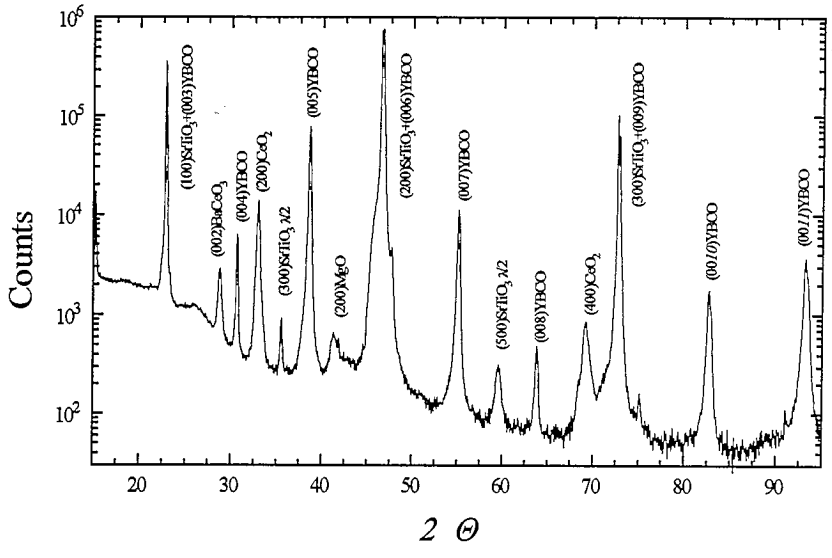

Fig. 1. Typical θ–2θ X-ray diffraction pattern obtained on an artificially engineered biepitaxial grain boundary structure fabricated under the processing conditions reported in Table 1.

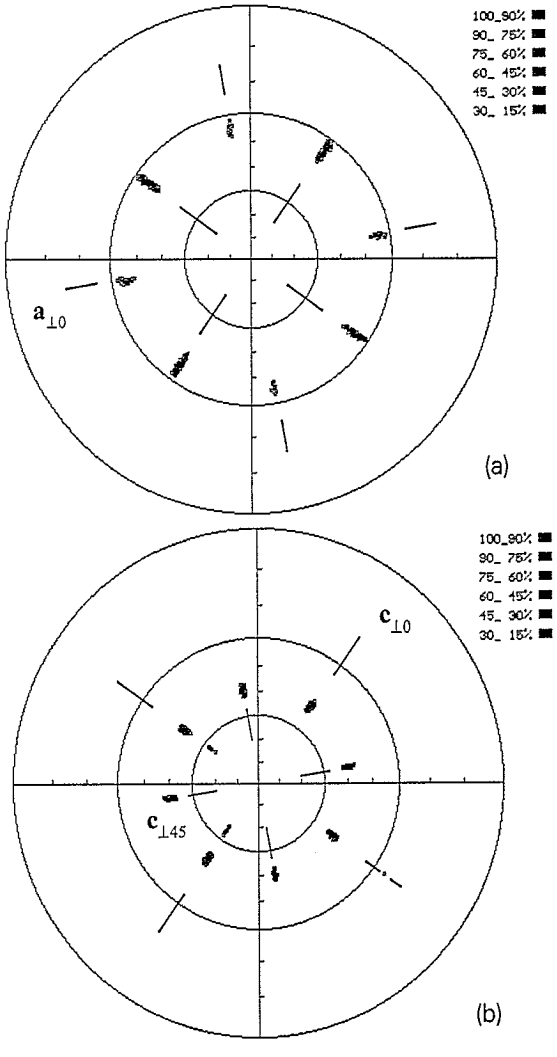

Fig. 2. $\{111\}_{CeO_2}$ (a) and $\{115\}_{YBCO}$ (b) pole figures for a bi-epitaxial grain-boundary structure. The eight-fold symmetry on both diffractograms indicate the occurrence of a 45° tilted grain boundary. After integrating over each set and averaging over a unit volume, the relative intensity ratios are $a_{\perp 0}^{CeO_2}/a_{\perp 45}^{CeO_2}=0.28$ and $c_{\perp 45}^{YBCO}/c_{\perp 0}^{YBCO}=0.87$ for $\{111\}_{CeO_2}$ and $\{115\}_{YBCO}$, respectively.

Two sets of 4 peaks located on a ring at $\chi=40°$ are clearly visible. The first set $C_{\perp 0}^{YBCO}$, stronger in intensity, has its poles almost aligned with the reference axes of the pole figure. The extension of each peak is 3° and 5° in φ and in χ, respectively. The second less intense peak set $C_{\perp 45}^{YBCO}$, detected at almost $\varphi=45°$ from the first set, shows a peak enlargement of 5° in both directions. Because of their proximity in the Bragg angle ($\theta_{102}^{STO}=27.16°$), two other peaks of $\{102\}_{STO}$, at $\chi\cong 25°$, and one peak of $\{201\}_{STO}$, at $\chi\cong 63°$, are also visible in this figure, showing the orientation of the underlying substrate. However, it is worth noting that, because of the relatively large experimental step here used, not all the $\{201\}_{STO}$ equivalent poles are visible.

From the occurrence of these two sets of peaks we can state that the YBCO film has two different heteroepitaxial relationships:

$$C_{\perp 45}^{YBCO}:\begin{cases}\langle 100\rangle_{YBCO}\|\langle 110\rangle_{CeO_2}\|(MgO)\|\langle 110\rangle_{STO},\\ \langle 001\rangle_{YBCO}\|\langle 001\rangle_{CeO_2}\|\langle 001\rangle_{MgO}\|\langle 001\rangle_{STO},\end{cases}$$

and

$$C_{\perp 0}^{YBCO}:\begin{cases}\langle 100\rangle_{YBCO}\|\langle 110\rangle_{CeO_2}\|\langle 100\rangle_{STO},\\ \langle 001\rangle_{YBCO}\|\langle 001\rangle_{CeO_2}\|\langle 001\rangle_{STO}.\end{cases}$$

The integration of the intensity over each set of poles per unit volume gives a relative ratio $C_{\perp 45}^{YBCO}/C_{\perp 0}^{YBCO}=0.87$ showing a slightly lower crystalline quality of the YCM side compared with the YC side. Further electron channelling pattern (ECP) analyses performed on a JSM 840-A scanning electron microscope confirm a lower texture of the $C_{\perp 45}^{YBCO}$. In fact, while the ECP analyses relative to the YC side are well comparable with those obtained on a perfectly heteroepitaxial single YBCO layer on perovskite substrates, we did not succeed in observing ECP images on the YCM side of the sample.

Fig. 3 reports a scanning electron microscopy picture of the region close to the grain boundary. Even if small voids are present on both parts of the sam-

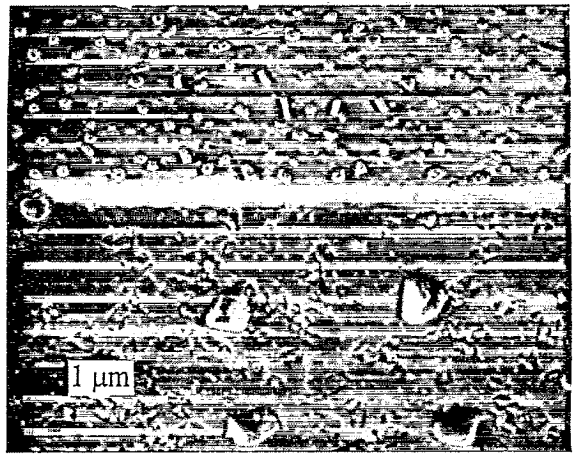

Fig. 3. Scanning electron microscopy image of a region close to the grain boundary.

ples, the larger structural disorder observed in the YCM part of the sample is correlated with a larger number of such imperfections. Some of them extend through the grain boundaries, making the film thickness irregular across the junction.

3.2. Electrical measurements

Fig. 4 displays the resistance (R) versus temperature (T) curves obtained on three different superconducting stripes defined across the grain boundary (□), on YCM (○) and on YC (◇) side of the sample. A 1 μA bias current on 10 μm wide stripes was used. While on the YC side of the sample the transition occurs at about 91 K, the lower T_c found in the YCM part reflects the structural disorder already found by X-ray analyses. On the other hand, the curve relevant to the stripe crossing the grain boundary shows two slopes. The voids found at the grain interfaces as well as some impurity phases correlated with them can account for the further lowering in the T_c. The inset in Fig. 4 shows a detail of each R versus $(T-T_c)$ curve near the transition. As indicated by the arrow, while the resistance of YCM and YC stripes suddenly reaches zero at the transition, that of the grain-boundary stripe drops down to about 2 Ω. We identify this residual resistance as the normal-state resistance of the junction defined by the stripe.

In Fig. 5, we report the I–V characteristics for a 10 μm wide junction at 9 K under microwave irradiation ($\nu_{RF}=8.822$ GHz) as a function of the incident power. Without irradiation the junction has a typical resistively shunted junction (RSJ) behavior with no hysteresis [17]. At this temperature we measure a critical current of about 100 μA corresponding to a current density of 5×10^3 A/cm^2. Moreover, the asymptotic resistance is $R_n=2.3$ Ω always below the transition temperature, giving an I_cR_n value of 230 μV. When microwaves are applied several Shapiro steps are displayed and, according to the Josephson relation $\Delta V=(h/2e)\nu_{RF}$, voltage steps separated by 18.3 μV are induced on the characteristics. The tested devices work up to 70 K showing Shapiro steps under microwave application over the whole operating range.

Fig. 6 shows the dependence of the current step heights, ΔI, as a function of the incident power for different temperatures. As expected from the RSJ model for low-impedance devices, we obtained the typical dependence for current-biased junctions [17] over the whole temperature range.

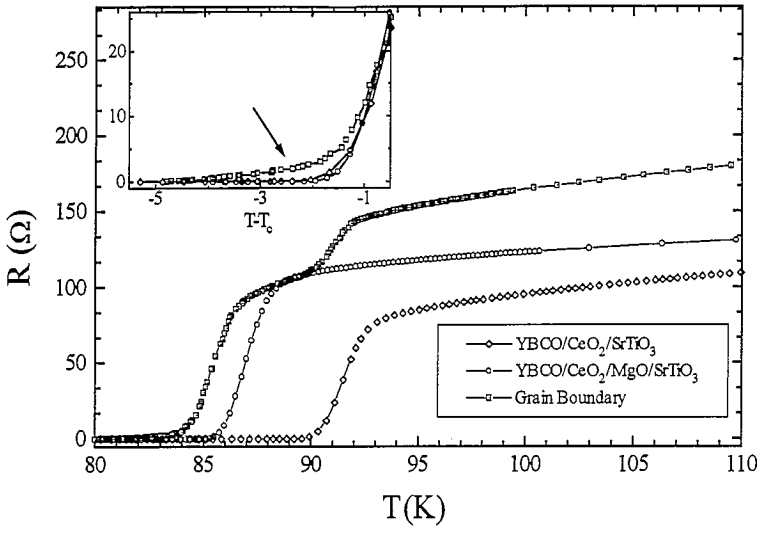

Fig. 4. Typical resistance vs. temperature curves obtained on three different superconducting stripes defined across the grain boundary (□), on the YBCO/CeO_2/MgO/$SrTiO_3$ (○) and on the YBCO/CeO_2/$SrTiO_3$ (◇) side of the sample. In the inset a detail of the R vs. $(T-T_c)$ curves near the transition. The arrow indicates the normal-state resistance of the junction defined by the strip patterned across the grain boundary.

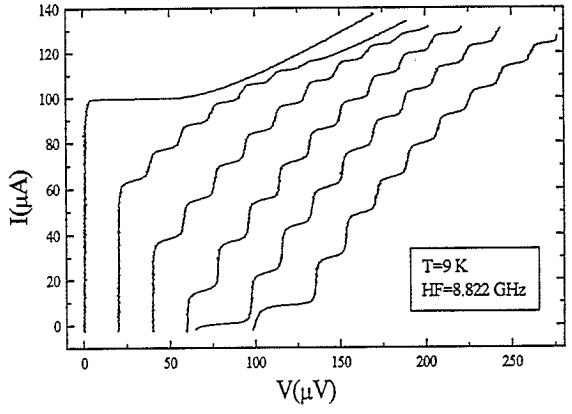

Fig. 5. I–V characteristics of a 10 μm wide 100 μm long junction under microwave irradiation as a function of the incident power.

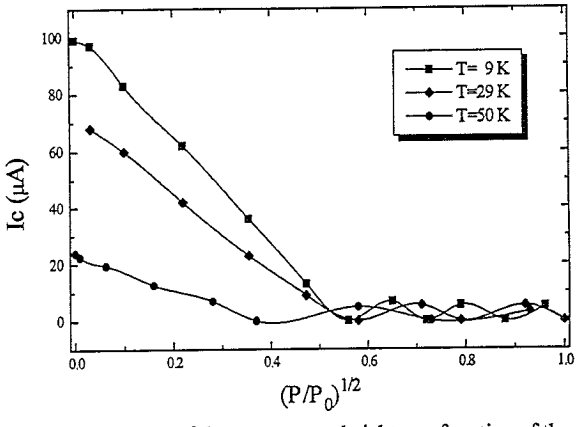

Fig. 6. Dependence of the current step height as a function of the incident power at different temperatures. The lines are simply a guide to the eye.

4. Conclusions

Artificially engineered bi-epitaxial grain boundaries were obtained by interposing a MgO seed layer between the STO substrate and the CeO_2 buffer layer. The overhanging YBCO film is slightly disordered with respect to the remaining part of the sample and the presence of the seed layer is correlated with the formation of several voids.

In spite of the presence of such voids at the grain boundaries, junctions fabricated on them show Josephson modulation in a wide temperature range and a I–V characteristic well described by the RSJ model behavior.

Acknowledgements

The authors wish to acknowledge M. Vabre and M. Levis for their skillful assistance in the device preparation and testing as well as F. Corticelli and D. Govoni for the useful assistance for the SEM image preparation.

This work was partially supported by ESPRIT Basic Research Action n. 7100: Grain Boundary Josephson Junctions in the High Temperature Superconductors (HTSC-GBJ).

One of the authors (SN) undertook this work by benefit of a grant from Consiglio Nazionale delle Ricerche (CNR): Comitato Nazionale per la Ricerca Tecnologica e l'Innovazione.

References

[1] J. Clarke, in: Superconducting Electronics, eds. H. Weinstock and M. Nisenoff, NATO ASI series. Series F: Computer and Systems Series, vol. 59 (Springer, Heidelberg, 1989) p. 87.
[2] B. David, in: European Training on Technologies and Industrial Application of Superconductivity, eds. A. Barone, A. Morini and L. Fruzio (World Scientific, Singapore, 1992) p. 159.
[3] S. Hontsu, N. Mukai, J. Ishii, T. Kawai and S. Kawai, Appl. Phys. Lett. 63 (1993) 1576.
[4] F. Pourtier and J.C. Villegier, in: Proc. OE/LASE '94, SPIE, vol. 2160, to be published.
[5] R. Gross, P. Chaudhari, D. Dimos, A. Gupta and G. Koren, Phys. Rev. Lett. 64 (1990) 228.
[6] J. Mannhart, P. Chaudhari, D. Dimos, C.C. Tsuei and T.R. McGuire, Phys. Rev. Lett. 61 (1988) 2476.
[7] R. Gross, P. Chaudhari, M. Kawasaki, M.B. Ketchen and A. Gupta, Appl. Phys. Lett. 57 (1990) 727.
[8] Z.H. Ivanov, P.Å. Nilsson, D. Winkler, J.A. Alarco, T. Claeson, E.A. Stepantsov and A.Ya. Tzalenchuk, Appl. Phys. Lett. 59 (1991) 3030.
[9] K. Char, M.S. Colclough, S.M. Garrison, N. Newman and G. Zaharchuk, Appl. Phys. Lett. 59 (1991) 733.
[10] L.P. Lee, K. Char, M.S. Colclough and G. Zaharchuk, Appl. Phys. Lett. 59 (1991) 3051.
[11] F. Wang, G. Kunkel, C. Coppetti, H. Kohlstedt and R. Wördenweber, in: Proc. EUCAS'93, ed. K. Sremyhrdt (DGM, Göttinger, 1993).
[12] J.C. Villegier, H. Moriceau, H. Boucher, R. Chicault, L. DiCioccio, A. Jäger, M. Schwerdtfeger, M. Vabre and C. Villard, IEEE Trans. Magn. 27 (1991) 1552.
[13] L.G. Schulz, J. Appl. Phys. 20 (1949) 1030.
[14] D. Chateigner, P. Germi and M. Pernet, J. Appl. Crystallogr. 25 (1992) 766.
[15] G.L. Skofronick, A.H. Carim, S.R. Foltyn and R.E. Muenchausen, J. Mater. Res. 8 (1993) 2785.
[16] X.D. Wu, L. Luo, R.E. R.E. Muenchausen, K.N. Springer and S. Foltyn, Appl. Phys. Lett. 60 (1992) 1381.
[17] A. Barone and G. Paternó, Physics and Applications of the Josephson Effect (Wiley, New York, 1982) p. 122.